Inorganica Chimica Acta 520 (2021) 120289

Contents lists available at ScienceDirect

Inorganica Chimica Acta

journal homepage: www.elsevier.com/locate/ica

Research paper

Sustainable photocatalytic synthesis of benzimidazoles

Tiziano Montini [a,b,*], Valentina Gombac [a,b], Juan J. Delgado [c], Anna Maria Venezia [d], Gianpiero Adami [a], Paolo Fornasiero [a,b]

[a] Department of Chemical and Pharmaceutical Sciences, INSTM Trieste Research Unit, University of Trieste, via L. Giorgieri 1, 34217 Trieste, Italy
[b] ICCOM-CNR Trieste, University of Trieste, via L. Giorgieri 1, 34217 Trieste, Italy
[c] Departamento de Ciencia de los Materiales e Ingeniería Metalúrgica y Química Inorgánica, Facultad de Ciencias, Universidad de Cádiz, Campus Río San Pedro, 11510, Puerto Real, Cádiz, Spain
[d] ISMN-CNR, Via Ugo La Malfa 153, 90146 Palermo, Italy

ARTICLE INFO

Dedicated to Dr. M. Peruzzini.

Keywords:
Photocatalysis
Benzimidazole
One-pot synthesis
Sustainability
Ethanol

ABSTRACT

Among the 17 Sustainable Development Goals presented by the United Nations in 2015, great attention is devoted to the production of goods and chemicals by use of renewable raw materials, by recycling of products and by extensive use of renewable energy sources. In this context, photocatalysis attracted great attention for the possibility to exploit Solar light to promote the desired chemical reactions. Besides its use in degradation of pollutants and in the production of fuels, some efforts have been devoted in the development of photocatalytic processes for the synthesis of fine chemicals with high added-value. In this work, we investigated the sustainable photocatalytic synthesis of benzimidazole derivatives through a one-pot, tandem process starting from a nitro compound and ethanol. By a photocatalytic approach, ethanol is dehydrogenated producing the hydrogen required for reduction of nitro groups and the aldehyde required for cyclization and production of the benzimidazole unit. Co-doping of TiO_2 with B and N is beneficial to increase the photocatalytic activity in H_2 production from ethanol. The effect of various metal co-catalysts (Pt, Pd Ag, Cu) have been evaluated on H_2 production rate and on selectivity in the synthesis of substituted benzimidazoles: Pt showed the highest selectivity in the desired products while Pd demonstrated a great activity for hydrodehalogenation, with potential interest for degradation of persistent pollutants.

1. Introduction

The demand for energy, food and goods of our modern society has been progressively increased in the last decades due to both the growth of world population and the improvements in life quality. The 12th of the 17 Sustainable Development Goals (SDG) adopted by the General Assembly of United Nation with the 2030 Agenda for Sustainable Development in January 2015 claims to "Ensure sustainable consumption and production patterns" [1]. The actions within this goal intend to favour sustainable exploiting of the natural resources, with extended recycling of materials and with favouring the transition from the use of fossil fuels to renewable raw materials.

The main beliefs of the 12th SDG and the principle of Green chemistry should be applied also in the production of fine chemicals with high-added value. In particular, the search of innovative production processes taking advantage of renewable reagents and energy sources represents an intriguing task for research in chemical sciences. In this context, photocatalysis is a key technology to promote chemical reactions using, in the best cases, solar light, a primary and renewable energy source, which is potentially well spread and largely available to everyone. Photocatalysis has been employed in the synthesis of organic compounds [2], pharmaceuticals [3] or of natural products [4]. Notably, in the majority of the studies, the photoactive component is a metal complex (based on Ru, Ir, Cu etc.) or an organic molecule (i.e. Eosin Y) [3,4]. These systems are usually working under visible light but suffer of the consequent problem of degradation of the molecular photoactive compound and of separation/recovery difficulties. Heterogeneous photocatalysts offers undoubtedly advantages of robustness and easy separation/recovery. Beside their well-known application in pollutants abatements from air or wastewaters, heterogeneous photocatalysis is obtaining promising performances in the production of solar fuels by valorisation of biomasses [5–8] and of liquid fuels from forestal/

* Corresponding author at: Department of Chemical and Pharmaceutical Sciences, INSTM Trieste Research Unit, University of Trieste, via L. Giorgieri 1, 34217 Trieste, Italy.
E-mail address: tmontini@units.it (T. Montini).

https://doi.org/10.1016/j.ica.2021.120289
Received 30 November 2020; Received in revised form 26 January 2021; Accepted 3 February 2021
Available online 12 February 2021

agricultural wastes [9]. In the chemical synthesis, in which high selectivity to the organic product is required, heterogeneous photocatalysts have been applied in reactions such as oxidation of benzylic alcohols [10–15], reduction of nitro compounds [14,16,17], functionalization of C—H bonds [15,18], Suzuki coupling [19,20] and others [2,21]. The weakness of this approach is its low selectivity. In fact, high selectivity to the desired product is typically obtained only when the molecular structure of the substrate is well defined.

The sustainability of chemical production will be further improved if heterogeneous photocatalysts will be applied in tandem processes, in which the same catalyst is employed to promote cascade reactions using solar light as primary energy source without the need to isolate the intermediate reaction products. A relevant example of this situation is the synthesis of benzimidazolic products from nitro compound. Benzimidazole and its derivative are fundamental building blocks in the synthesis of natural products and pharmaceuticals [22], showing biological activity mainly as bactericides [23], anticarcinogens [24] and peptic ulcera agents [25]. Moreover, benzimidazoles are used as ligands in metal complexes [26–28], that are employed in catalysts and sensors. The synthesis of benzimidazoles is classically performed by coupling 1,2-arylenediammine with aldehydes, carboxylic acids or their derivatives [29–33], requiring medium – high temperatures (100–200 °C) and often strong oxidants. To overcome these harsh conditions, Shiraishi et al. reported an one-pot method in which 1,2-phenylenediammines are coupled with aldehydes produced by photocatalytic dehydrogenation of alcohols using Pt/TiO_2 under UV–vis irradiation ($\lambda > 300$ nm, Xe lamp, 2 kW) [34]. The photocatalyst is involved in both the dehydrogenation of alcohol to produce the required aldehyde and in the dehydrogenation of the intermediates, necessary to obtain the final benzimidazole products. Notably, the most important by-products reported in this paper are N-substituted-2-alkyl-1H-benzimidazoles. Although this method allows the preparation of 2-substitured 1H-benzimidazoles under very mild conditions, it does not overcome the important safety problem related with the employment of highly toxic compounds, such as 1,2-arylenediammine. In a subsequent study, Selvam and Swaminathan [35] reported the first example of an one-pot synthesis of benzimidazoles from nitrocompounds in alcoholic solvent, using the dehydrogenation of the alcohol to reduce the $–NO_2$ to $–NH_2$ and produce the aldehyde required for the synthesis of the cyclic compound. Anyway, this work shows important limitations. First, the photocatalyst employed (Pt/TiO_2) is irradiated with a monochromatic UV light at 365 nm. Second, the nitrocompounds employed are N-substituted 2-nitro arenes, in which the amino group is already bearing a substituent. This was done in order to reduce the number of possible by-products obtained in the reaction. Despite these limitations, the work by Selvan and Swaminathan [35] represents the elegant attempt to combine more reaction steps into a single one-pot photocatalytic process.

A key step in the tandem synthesis of benzimidazoles is the efficient hydrogen abstraction from alcohols. Dehydrogenation of alcohols to produce H_2 is a well know process [5,7,36] and, in our research group, great efforts have been dedicated to the development of TiO_2-based photocatalysts able to harvest solar light extracting H_2 from renewable raw materials like ethanol [37–45] and glycerol [38,39,42–44,46,47]. Activity of TiO_2 materials can be further improved by doping, in order to modify the electronic properties of the semiconductor. Doping results usually in increasing on solar light harvesting and/or in increasing the lifetime of photogenerated e-/h + couples [49].

In this work, we investigated the tandem, one-pot synthesis of 1H-benzimidazoles starting from nitro compounds (1,2-dinitrobenzene or substituted 2-nitroaniline) by a photocatalytic approach, in which ethanol acts as source for the hydrogen, required in the reduction of nitro groups, and for the aldehyde, required in the cyclization process. The main product of this process is a 2-methyl-1H-benzimidazole (2-MBI). In this research work, we investigated the photocatalytic performances in ethanol dehydrogenation of TiO_2 co-doped with B and N and of the nature of various metal co-catalysts. The most promising photocatalysts have been studied for the one-pot synthesis of 2-MBI. The experimental conditions (nitro compounds used as precursor, solvent) have been optimized using 2-nitroaniline. Finally, the effect of the metal co-catalyst in the product selectivity has been evaluated for the synthesis of substituted 2-MBI, in order to obtain products that can be further functionalised on the aromatic ring and, therefore, interesting for synthesis of more complex molecules.

2. Experimental section

2.1. Catalyst preparation

TiO_2 and TiO_2-B,N supports were prepared following a sol–gel approach. Briefly, two solutions were rapidly mixed: the first solution was made by *tert*-butyl orthotitanate dissolved in absolute ethanol (1.7 M) while the second contains H_2O and nitric acid (as catalyst). In the case of TiO_2-B,N, H_3BO_3 (in 9:100 M ratio with respect to Ti) and urea (in 5:100 M ratio with respect to Ti) were added simultaneously in the second (aqueous) solution. After dropping the ethanolic solution containing the Ti precursor into the aqueous solution under gentle stirring, a gel was obtained in a few minutes. The gel was aged for 24 h at room temperature, dried at 120 °C for 12 h and finally calcined in a static oven at 450 °C for 6 h.

Metal co-catalyst (Pd, Pt, Ag, or Cu) was deposited on the surface of the supports by a simple photodeposition technique starting from a water/methanol solution of correspondent nitrate salt. Briefly, 500 mg of the support was suspended into 120 mL of water/methanol solution containing an adequate amount of the metal precursor in order to reach the desired metal loading (0.5 wt% for Pd, Pt, and Ag and 1.0 wt% for Cu). After equilibration in the dark for 30 min, the suspension was irradiated with UV–vis light (125 W Hg medium pressure lamp, Helios) for 2 h. Finally, the solid was recovered by filtration and dried in an oven at 80 °C for 12 h, without any further treatment.

2.2. Sample characterization

Textural properties of the samples were characterized by N_2 physisorption at the liquid nitrogen temperature using a Micromeritics ASAP 2020 porosimeter. Before the analysis, the samples have been degassed at 120 °C overnight.

Powder X-ray diffraction patterns were collected using a Philips X'Pert diffractometer, using Cu Kα radiation. Cu $K\alpha_2$ was removed by computer-processing of the data. Phase analysis was performed using the Rietveld method through the PowderCell 2.0 program while mean crystallite size was calculated applying the Scherrer's equation to the main reflection of each phase.

UV–vis spectra of solutions were collected using a Shimadzu Shimadzu UV-2450, acquiring absorbance in the range 300 – 800 nm.

ICP-OES analysis has been performed using an Optima 8000 Spectrometer (PerkinElmer) equipped with a S10 autosampler. The total copper concentration was evaluated using calibration curves obtained by dilution of SpectrascanTM copper standard solutions for ICP-OES analysis (Teknolab A/S, Norway). All standards (range: 0.1–50.0 mg/L) were prepared using a EtOH 96% solution to compensate the matrix effect. The used emission wavelength was 324.754 nm, the limit of detection 0.03 mg/L and the repeatability of measurements expressed as relative standard deviations (RSD%) and calculated on 6 replicates of various samples was lower than 4%. Calibration curves obtained by means of 5 standard solutions had correlation coefficients higher than 0.998.

The samples were characterized by means of High Resolution Electron Microscopy (HREM) on a JEOL2010 field emission gun microscope operated at 200 kV and with a spatial resolution of 0.19 nm at Scherzer defocus conditions. In order to obtain the particle size distribution and chemical information of the sample, High Angle Annular Dark Field-Scanning Transmission Electron Microscopy (HAADF-STEM)

technique, in combination with X-Ray Energy Dispersive Spectroscopy (X-EDS, Oxford Instrument), was used. These experiments were carried out at the same microscope using an electron probe of 0.5 nm of diameter and a diffraction camera length of 10 cm. The sample was deposited on a Cu grid covered with a thin layer of holey carbon (Ni grind in the case of Cu/TiO_2-B,N).

The X-ray photoelectron spectroscopy (XPS) analyses of the powder samples were performed with a VG Microtech ESCA 3000 Multilab, using Al Kα radiation (1486.6 eV) from a dual Mg/Al anode. The constant charging of the samples was corrected by referencing all the binding energies to the C 1 s peak energy set at 285.1 eV, arising fom adventitious carbon. Qualitative and quantitative analyses of the peaks were performed with the CasaXPS software.

UV–vis diffuse reflectance spectra were measured on a Varian Cary 4000 UV–vis spectrophotometer equipped with an integrating sphere. Spectra were collected in the range of 200 – 800 nm. MgO was used as a white standard material. Band gap energies were determined by constructing Tauc plots for an indirect semiconductor from the calculated Kubelka-Munk functions of the respective diffuse reflectance spectra.

Produced H_2 has been quantified using a gas-chromatograph Agilent 7890 mounting a TCD detector connected with a Supelco Carboxen 1010 column (30 m, 0.52 mm ID, 0.5 μm film) with Ar as gas carrier. Volatile products (by-products from ethanol dehydrogenation and various benzimidazoles) were analysed GC/MS Agilent 7890 GC equipped with an Agilent 5975C mass spectrometer and mounting a J&D DB-225 m column (60 m, 0.25 mm ID, 0.25 μm film) and using He as carrier.

2.3. Photocatalytic tests

Photocatalytic activity experiments were performed using a Solar Simulator (LOT-Oriel) equipped with a 150 W Xe lamp and an Atmospheric filter (cut-off at 300 nm), in order to simulate the radiation that reaches the Earth surface. The radiation intensity reaching the reactor, as measured with a radiometer (Delta Ohm HD 2302.0 LightMeter), was 25 mW/cm^2 in the UV-A range (315–400 nm) and 180 mW/cm^2 in the vis-NIR range (400–1080 nm). This situation corresponds to a powder density around 2 Suns, typical of a small solar concentrator.

A semi-batch reactor, equipped with a glass window, was used for photocatalytic experiments. In H_2 production studies, 150 mg of the photocatalysts were suspended into 60 mL of ethanol 96% (commercial azeotropic mixture) and the reactor temperature was controlled at 30 °C using a thermostatic water bath. After purging the reactor with Ar (15 mL/min) for 30 min, the lamp was switched on and on-line analysis of the H_2 produced and transferred by the Ar flow (15 mL/min) to the GC.

Apparent quantum yields (AQY) were measured using the same apparatus. After 3 h for activation of the photocatalysts and to reach steady-state conditions, a 10 nm bandpass filter centred at 350 nm was inserted obtaining an irradiation power of 2.78 mW/cm^2. H_2 production was monitored for at least other 12 h, in order to reach a stable value. Considering that 2 electrons are required to produce one H_2 molecule, AQY was calculated following the formula:

$$\mathrm{AQY} = \frac{2 \text{ x number of } H_2 \text{ molucules}}{\text{number of incident photons at 350 nm}}$$

Synthesis of benzimidazoles was performed suspending 150 mg of catalyst into 60 mL of a 4 mM solution of precursor in ethanol–water solution (with different composition). After purging with Ar for 30 min, lamp was switched on and small portions of the suspension were collected every hour to check the progress of the reaction by UV–vis analysis and/or GC/MS analysis (after filtration of the catalyst). During irradiation, Ar effluent was periodically analyzed to check the presence of gaseous products by GC: experiments were stopped when H_2 was detected in the gas phase. Various experiments have been performed to evaluate the effect of metal co-catalyst and water amount in the solvent on yield and selectivity on desired benzimidazole.

For the selectivity tests with substituted 2-nitroanilines, experiments were performed in the same conditions in ethanol 96% without sampling. At the end of the synthesis, the catalyst was removed by filtration and solvent has been evaporated under vacuum. The crude mixture containing the benzimidazole products were dissolved in 15 mL of HCl 5% and extracted with CH_2Cl_2 (3 × 10 mL) to remove organic contaminants. Then, the aqueous solution was neutralized with NaOH and extracted with CH_2Cl_2 (3 × 10 mL) to extract the benzimidazole products. After drying on Na_2SO_4 and evaporation to dryness under vacuum, the product was dissolved in 2 mL of methanol for GC/MS analysis.

3. Results and discussion

3.1. Characterization of the catalysts

After preparation, the TiO_2 based materials have been characterized to gain information on phase composition and textural properties. Powder XRD analysis (Fig. 1) showed that the obtained materials are multiphasic, comprising a mixture of anatase, brookite and rutile. The phase composition has been determined by Rietveld analysis of the XRD patterns presented in Fig. 1 and the quantitative results (summarized in Table 1) show that the relative amounts of the three phases are not affected by the introduction of B and N as co-dopants for TiO_2. The cell parameters of the 3 phases are only marginally affected by the introduction of the co-dopants (see Table S1), in agreement with the low loading of B and N in the TiO_2-B,N material. On the other hand, a significant reduction of average crystallite size has been observed for all the phases, in particular for the rutile polymorph. This effect has been already observed for TiO_2 material doped with non-metal elements [50,51].

As a result of the reduction of crystallite size, the textural properties of the materials are strongly affected by the addition of dopants. Both the materials present a Type IV isotherm (Fig. S1a), typical of mesoporous material [52]. The large hysteresis of Type H2 (Fig. S1a) is indicative of the presence of bottled-neck pores [52]. Despite these general similarities, the specific surface area and the cumulative pore volume of TiO_2-B,N are much larger than that of the corresponding undoped TiO_2 (Table 1 and Fig. S1b). At the same time, the maximum of the pore size distributions (from the BJH analysis of the desorption branch of the isotherms, Fig. S1c) is shifted to slightly smaller diameter in the case of the doped material. All the modification in textural properties are clearly related with the different aggregation of crystallites depending on their sizes.

These important differences in structural and textural properties of TiO_2 and TiO_2-B,N could be easily related with the presence of the dopants. The detection of B and N into TiO_2 matrix is not a simple task, considering that both are light elements. Moreover, it is know that calcination treatments in air are able to remove the most part of them [51]. In our case, XPS has been employed to reveal the presence of B and N in the TiO_2-B,N material (spectra reported in Fig. S2). Despite the fact that XPS is a surface-sensitive technique, the results clearly reveal that B is actually present in the sample: the position of B 1 s signal (192.70 eV) is typical of species of B interacting with O, like H_3BO_3 or B_2O_3 [53]. Ti 2p signal shows the typical bands on Ti^{4+} in TiO_2 while O 1 s can be deconvoluted into 2 peaks, related with O in TiO_2 (530.01 eV) and in B_2O_3 (531.80 eV) [53]. The atomic contents of B and Ti revealed by XPS are 7.03 at% and 29.02 at%, which correspond to a B/Ti ratio of 0.242 that is much higher that the nominal B/Ti ratio of 0.09 employed during the synthesis. This suggests that B is mainly segregated in the outermost layers of TiO_2 nanocrystals and can justify the different sintering behaviour of the TiO_2-B,N with respect to undoped TiO_2, finally leading to higher surface area for the doped material. Notably, no signals can be distinguished from the background in the region of binding energy of the N 1 s (396 – 410 eV). This result suggests that the most part of N has been removed during the calcination treatment at the end of sol–gel synthesis or, if present, it is located mainly in the bulk of the material.

The optical properties of TiO_2 and TiO_2-B,N has been characterized

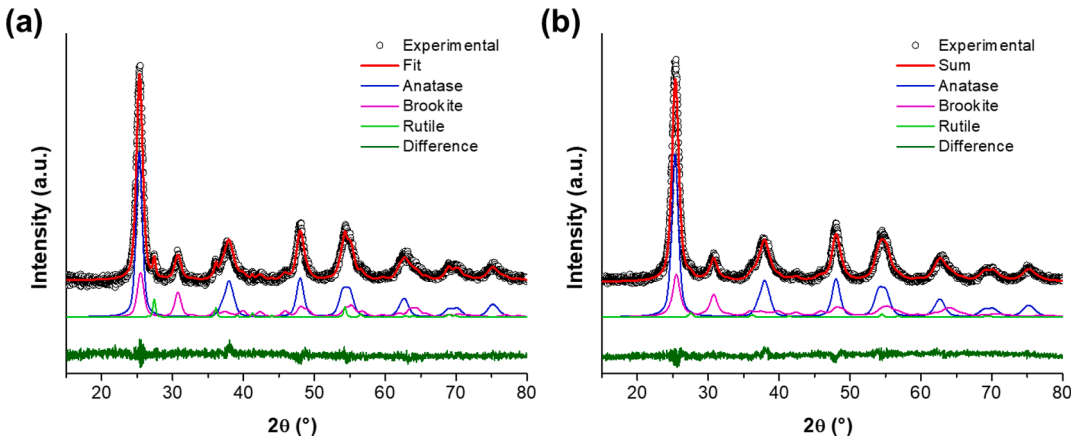

Fig. 1. Powder XRD patterns of (a) TiO_2 and (b) TiO_2-B,N supports.

Table 1
Structural and textural characteristics of TiO_2 and TiO_2-B,N photoactive materials.

	Composition (wt%)			Crystallite size (nm)			SSA (m^2/g)	CPV (mL/g)	d_M (nm)
	A [a]	B [a]	R [a]	A [a]	B [a]	R [a]			
TiO_2	64	28	8	11	11	32	80	0.149	6.8
TiO_2-B,N	69	27	4	8	7	12	138	0.276	6.3

[a]A = anatase; B = brookite; R = rutile.
[b]SSA = Specific surface Area; CPV = Cumulative Pore Volume; d_M = maximum of the pore size distribution obtained from BJH analysis of the desorption branch of the N_2 physisorption isotherm.

by diffuse reflectance UV–vis spectroscopy. As expected, the two photoactive materials show photon absorption only in the UV range, below 400 nm (Fig. S3a). By extrapolation of the linear parts of Tauc plots (Fig. S3b), indirect band gaps of 2.96 and 2.97 eV were calculated for TiO_2 and TiO_2-B,N, respectively. These results are in good agreement with experimental [51] and theoretical [49,54] studies regarding the effect of B doping on the electronic structure of TiO_2: with its low nuclear charge, the electronic 2p states of B are located at energy higher than the lower edge of conduction band of TiO_2 (made essentially by 3d states of Ti) [49,54]. As a consequence, band-gap band gap is marginally affected by B doping. On the other hand, a decrease in band gap was expected by doping with N [49,51,54], since N introduces filled 2p states just above the top of the valence band (made essentially by O 2p states). This effect was not observed in TiO_2-B,N since the amount of N dopant is negligible (if present).

The morphology of the photocatalysts has been investigated by means of HAADF-STEM. The results are summarized by the representative images presented in Fig. 2 while the size distribution of the metal nanoparticles are compared in Fig. 3. TiO_2-B,N is composed by an agglomeration of crystallites of TiO_2 with an irregular shape and crystallite sizes in the range 5 – 20 nm, in agreement with the results obtained from the powder XRD.

Metal nanoparticles can be easily observed by HAADF-STEM on the surface of TiO_2-B,N, even if with different contrast (Fig. 2). The size distributions of metal nanoparticles strongly depends on the type of metal. The mean size of the Pt and Cu nanoparticles is around 2 nm, with a narrow distribution. This is in agreement with previous observation on similar materials [38,44]: the small metal nanoparticles have been formed by reduction of metal ions through the electrons excited in the conduction band. In this way, many nucleation centres are formed and nucleation results faster than growth of metal nanoparticles. On the

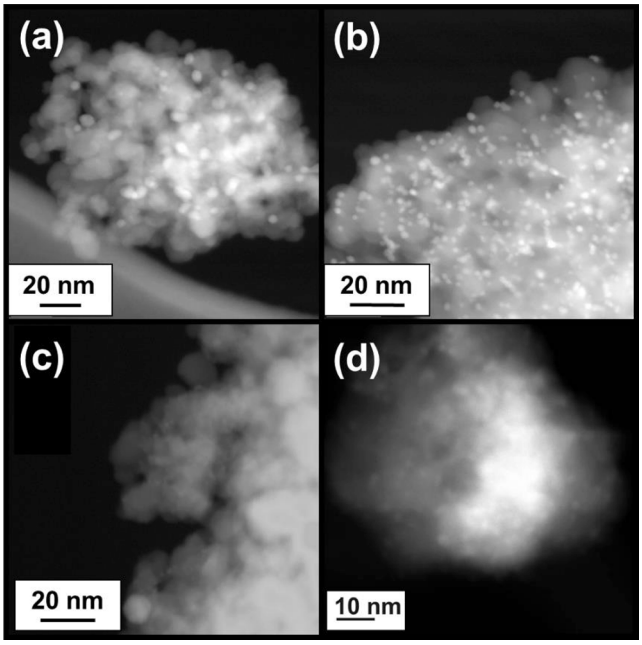

Fig. 2. Representative HAADF-STEM micrographs of the photocatalysts based on TiO_2-B,N after photodeposition of the metal cocatalysts: (a) Pd 0.5 wt%, (b) Pt 0.5 wt%, (c) Ag 0.5 wt% and (d) Cu 1.0 wt%.

other hand, Pd and Ag show very broad size distributions, with the presence of few very large metal nanoparticles (up to ~ 40 nm for Ag). A rare image of this situation is presented in Fig. S4, in which a very large Ag particle is present together with many small nanoparticles. In these cases, it is evident that growth rate becomes competitive with nucleation rate, even if similar amounts of photogenerated electrons are expected for all the samples supported on TiO_2-B,N. These results are in good agreement with the recent study of Puga et al. [55]. As a comparison, Pd/TiO_2 has also been analysed by HAADF-STEM (Fig. S5). The broad distribution of Pd nanoparticle sizes obtained also in this case suggests that, when Pd is photodeposited, the growth process is competitive with the nucleation process without an evident dependence from the doping of the TiO_2 support.

3.2. *Photocatalytic H_2 production*

With the aim to use H_2 produced in situ for the subsequent reduction of nitro groups, the prepared catalysts have been preliminary tested for the photocatalytic H_2 production from aqueous solutions containing

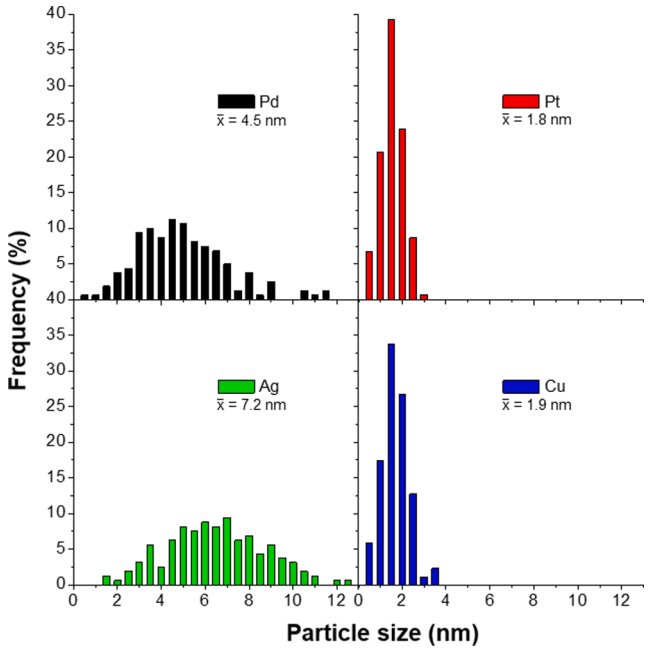

Fig. 3. Size distribution of the metal nanoparticles in TiO_2-B,N samples with photodeposited metal co-catalysts. Approximatively 400 particles were counted for each distribution.

EtOH as sacrificial agent. The tests have been performed to confirm the positive role of the co-doping and the effect of the type of metal on the rate of H_2 production.

Under the adopted experimental conditions, the photocatalytic H_2 production takes place mainly by dehydrogenation of ethanol to acetaldehyde [7,38,44,45,57]. The GC/MS analysis of the liquids collected at the end of each experiment always show the presence of acetaldehyde and 1,1-diethoxyethane, the acetal formed by acetaldehyde and excess ethanol (Fig. S6). Moreover, no detectable amounts of CO, CO_2 or CH_4 have been observed in the gas effluents from the photoreactor. Typically, H_2 production starts immediately but a progressive increase is observed in the first hours due to the chromatographic effect within the reactor. As the only exceptions, Cu-based photocatalysts show an activation period (Fig. 4 and S7), with H_2 production becoming significant only after 1.5 h of irradiation. The delay in H_2 production at the beginning of the experiments is due mainly to 2 effects: stabilization of H_2 concentration in the dead volume of photoreactor and activation of the photocatalyst. In the case of Pt, Pd and Ag co-catalysts, metal nanoparticles (deposited in the zero-valent state during preliminary photodeposition) maintain their conditions, being immediately available to promote H_2 production. Therefore, in these cases, initial delay is due only to H_2 diffusion in the dead volume of photoreactor. In the case of Cu/TiO_2-B,N, it is demonstrated that Cu nanoparticles produced by photodeposition are rapidly oxidized by exposure to air [38,55]. In this case, a longer time is needed to reach a stable H_2 production since photogenerated electrons are consumed to reduce CuOx species to Cu nanoparticles before H_2 production begins [38,55,58–61]. Various reports in the literature assess that photocatalysts comprising nanocomposite made by different TiO_2 polymorphs are more active than the single phase materials both in oxidation [62,63] and in reduction [64–66] processes. This is due by the formation of heterojunctions between the crystallites of the different phases and the capability of photogenerated electrons and holes to transfer from phase to phase. Considering this, electron/hole recombination is highly inhibited in multiphasic TiO_2, leading to a higher number of sites for nucleation of metal nanoparticles, essential to have a high rate of H^+ reduction to H_2, and for oxidation of the molecules of the sacrificial agent.

The obtained experimental data indicate that both the composition of the photoactive material and the nature of the co-catalyst strongly affect the activity. In particular, the H_2 production is enhanced by co-doping of TiO_2 with B and N (Fig. 4a for Pd-based photocatalysts), as a result of more efficient light harvesting, increased life-time of photogenerated h^+/e^- pairs and increased surface area [49–51,67,68]. The same trend has been observed for Cu-based photocatalysts (Fig. S7). Normalizing the H_2 production rate with respect to the surface area (Fig. S8), the photocatalysts supported on undoped TiO_2 show a higher efficiency in H_2 evolution with respect to the materials prepared using TiO_2-B,N. It must be underlined here that the experimental conditions employed in the H_2 production tests are optimized for the forthcoming benzimidazole synthesis: the optimal amount of TiO_2 photocatalyst, accordingly to [69], is around 60 mg [38,44] instead of the 150 mg employed here. In this work, the amount of H_2 produced and available for nitro groups reduction has been estimated and the most part of the catalyst will be required for the "dark" steps involved in bezimidazole synthesis (see below).

More relevant is the effect of metal employed as co-catalyst (Fig. 4b). Among the studied metals, the best performances was observed by Pt and Pd followed by Cu that showed higher H_2 production rate than Ag. This trend is in agreement with previous reports on the effect of work function of the metal co-catalyst on H_2 production rate in photocatalytic experiments [70–72]. It was demonstrated that higher is the work function, higher is the Schottky barrier formed at the interface between metal nanoparticles and semiconductor. As a result, e^-/h^+ pairs recombination is strongly inhibited, favouring their redox processes taking places on the surface of the photocatalyst, like proton reduction to H_2 and oxidation of the adsorbed ethoxy groups to acetaldehyde [7].

Notably, Cu-based photocatalysts suffer of some metal leaching during photocatalytic experiments, even under reducing conditions like in the case of H_2 production from alcohol dehydrogenation [38,39]. In the present case, Cu concentration in the liquid phase at the end of photocatalytic H_2 production experiments has been measured by ICP-OES. The amount of Cu detected in solution corresponds to 16.1 wt% of the nominal Cu introduced into the reactor for Cu/TiO_2 while this quantity decreases to 5.9% for Cu/TiO_2-B,N. This significant reduction is very important in view of a practical application of this type of photocatalysts. The reduction of Cu leaching could be due to the combination of different factors, including an increase of the surface area, the presence of different basic sites due to the presence of dopants that favour the adsorption of Cu(II) ions and/or the modification of valence band edge that hinder re-oxidation of metal nanoparticles. Reasonably, Cu leaching could be further reduced employing a light source with a larger fraction of UV photons [39].

Apparent quantum yields for H_2 production under the present conditions have been estimated irradiating the samples based on TiO_2-B,N with UV light around 350 nm, by the use of a 10 nm bandpass filter. The results (Fig. S9) clearly show that, under "monochromatic" irradiation in the UV range, the H_2 production rates are obviously lower because of the lower total number of photons but follow the same trend presented in Fig. 4b. Apparent quantum yields are in the range 1.7 – 6.5%, in agreement with previous reports on the use of TiO_2-based photocalysts for H_2 production from alcohols [74,75].

On the bases of the discussed positive textural characteristics (larger surface area) and promising photocatalytic H_2 production of TiO_2-B,N the subsequent studies on the photocatalytic synthesis of benzimidazolic compounds were performed on those materials only.

3.3. *Photocatalytic synthesis of benzimidazole: influence of reaction conditions*

The experimental conditions for the synthesis of benzimidazolic compounds have been first optimized using Pt/TiO_2-B,N photocatalyst. Notably, the amount of photocatalyst employed is much larger than that optimized for photocatalytic H_2 production from ethanol solution, since TiO_2-B,N must provide also sufficient acid sites to catalyse the

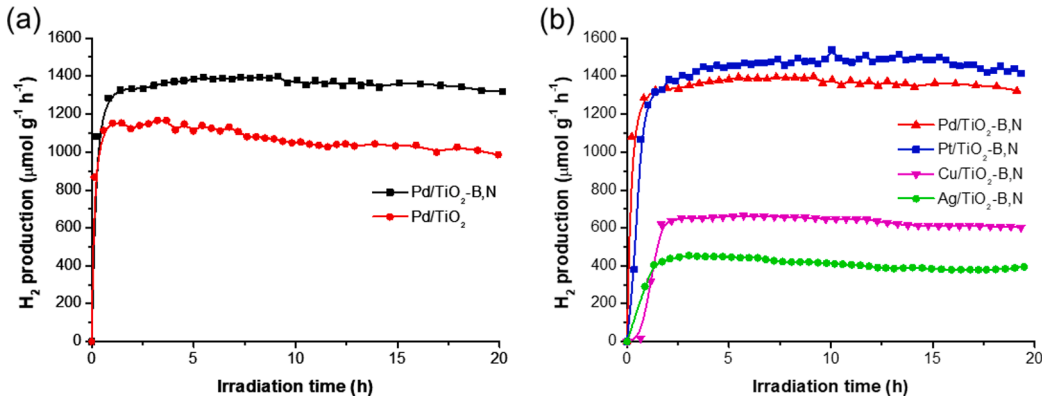

Fig. 4. H_2 production rate during photocatalytic dehydrogenation of ethanol: (a) effect of doping on TiO_2 and (b) effect of metal co-catalyst.

condensation and cyclization steps.

The proposed reaction scheme is presented in Fig. 5. It starts with the production of H_2 and aldehyde by alcohol photoassisted dehydrogenation, followed by in situ reduction of a nitro compounds to an intermediate phenylenediamine, that is finally condensed with the aldehyde forming an imine compounds. This intermediate undergoes rapid cyclization and the desired product is obtained by oxidation/dehydrogenation. Even if often carboxylic acids or their derivatives have been employed in the synthesis of benzimidazoles, in this mechanism the oxidation of acetaldehyde has been excluded considering that:

- Oxidation of acetaldehyde has never been observed under the experimental conditions adopted in this study [38,44];
- Formation of benzimidazoles from aldehydes requires very mild conditions, like those employed in this study [33].

The initial tests has been performed using 2-nitroalinine (NA) or 1,2-dinitrobenzene (DNB) as starting compounds and ethanol as alcohol, being 2-methyl-1H-benzimidazole (2-MBI) the expected product of the reaction.

The results obtained during irradiation of DNB in EtOH 96% in the presence of Pt/TiO_2-B,N photocatalyst are presented in Fig. 6a. The synthesis of 2-MBI from DNB in EtOH 96% showed that the precursor starts to be consumed immediately after beginning of irradiation of the photocatalyst. The molar fraction of DNB progressively decreased with the complete conversion achieved around 17 h. During this period, the molar fraction of NA increased rapidly in the initial 2 h up to 30 – 40%, maintaining in this range until DNB is totally consumed; after that, NA amount decreased, being reduced and converted into the benzimidazolic product. During all this period, the molar fraction of 2-MBI progressively increased. A similar trend has been observed also analysing the UV–vis spectra of the solutions collected during the synthesis (Fig. S10). After switching on of the lamp, a band related to NA and centered around 406 nm appears, with intensity increasing in the first hours and then quickly disappearing after 18 h. At the same time, the bands related to 2-MBI (sharp bands in the range 250 – 300 nm) progressively increases. The H_2 evolution is very low during 18 h of irradiation but, after this period, a sharp increase in the H_2 production is observed, in concomitance with the decrease in NA amount. The steeply increase in H_2 production rate corresponds to the complete reduction of nitro groups. This scenario suggests that the pathway followed to produce the 2-MBI product starts with the reduction of DNB to NA (Fig. 5). At this point, NA can be reduced to 1,2-phenylenediamine, which quickly undergoes condensation with acetaldehyde (produced from ethanol dehydrogenation). The formation of the mono-imine derivate is crucial for the following cyclization/dehydrogenation to 2-MBI. Notably, no 1,2-phenylenediamine has been detected by GC/MS analysis of the aliquots sampled during the experiment indicating that, under the present conditions, cyclization reaction is very fast with respect to reduction of the nitro groups and all the equilibria involved in imine formation are shifted to the products. Together with 2-MBI, other two compounds have been detected in GC/MS analysis as by-products: 1-*N*-(1-ethoxyethyl)-2-methyl-1H-benzimidazole (*N*-EtOEt-2-MBI, 5.3 mol%) and 1-*N*-ethyl-2-methyl-1H-benzimidazole (*N*-Et-2-MBI, 3.1 mol%). Their formation is clearly related with the accumulation of acetaldehyde from ethanol dehydrogenation, which favours the formation of the di-imine intermediate that, after various steps involving cyclization, dehydrogenation and reaction with the solvent, produces the *N*-substituted 2-MBI. A plausible pathway for the obtainment of the *N*-substituted 2-MBI is presented in Fig. S11 and involves also the catalysis by acid sited of TiO_2

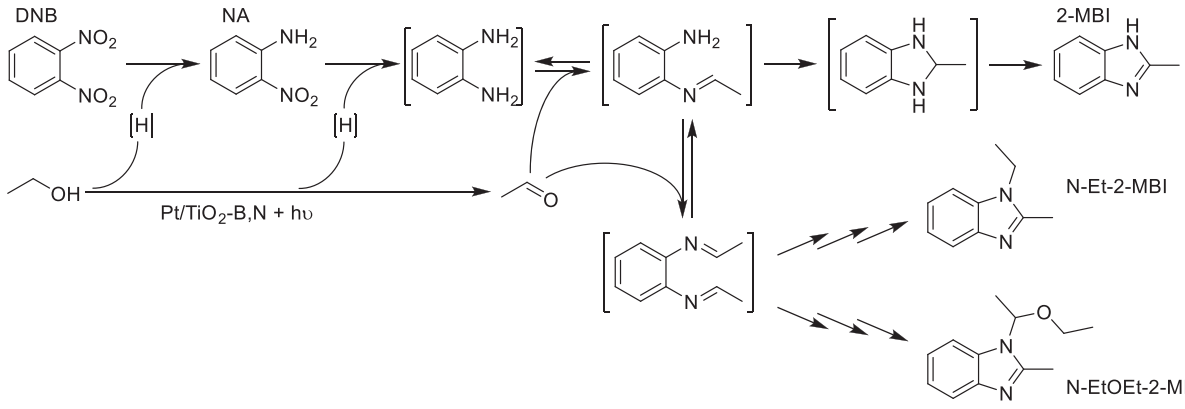

Fig. 5. Possible reaction pathway for the photocatalytic production of the 2-MBI from DNB and/or NA coupled with photocatalytic dehydrogenation of ethanol. The intermediates within square brackets have net been detected by GC/MS analysis (see text).

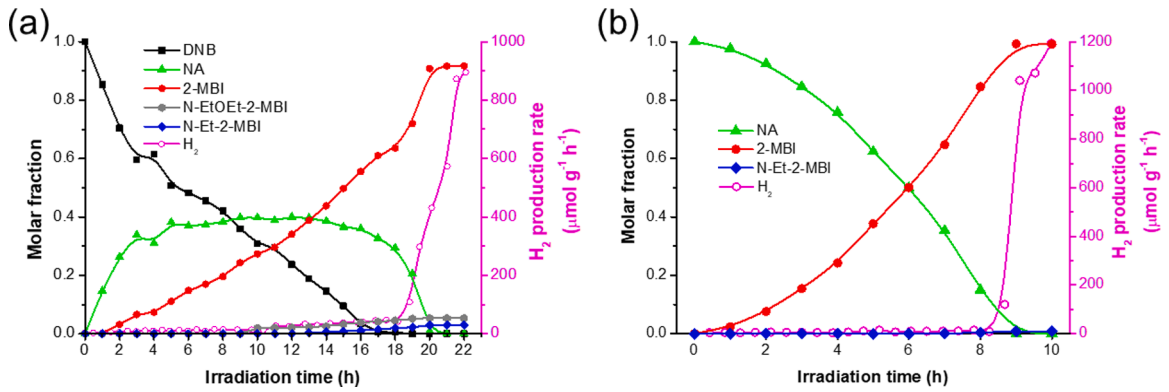

Fig. 6. Photocatalytic synthesis of 2-MBI using DNB (a) or NA (b) as starting molecule. Experimental condition: 150 mg Pt/TiO_2-B,N, 60 mL solution of precursor 4 mM in EtOH 96%, 30 °C, 30 mL/min Ar flow, simulated sunlight irradiation.

and the ability of Pt nanoparticles to promote hydrogenation/dehydrogenation.

Efforts to reduce the formation of these by-products is mandatory. Therefore, we studied the influence of the presence of H_2O in the solvent on the imine formation equilibrium. In fact, an optimized amount of water could reduce and even avoid the formation of the di-imine intermediate. The results obtained varying the H_2O amount from 0 to 20 vol% in the solvent are presented in Fig. S12. In the absence of H_2O, the main by-product is *N*-EtOEt-2-MBI (19.6 mol%) followed by *N*-Et-2-MBI (3.3 mol%). Adding a large amount of H_2O (20 vol%), the main by-product observed is 1,2- phenylenediamine (10.4 mol%), suggesting the incomplete conversion into benzimidazoles as an effect of shifting the equilibrium reaction of imine formation to the reagents. As observed, the optimal amount of H_2O for benzimidazole formation is between 4 and 10 vol%. The by-products cannot be totally eliminated since the acetaldehyde concentration increases due to the high amount of H_2 required for the reduction of 2 nitro groups. Notably, it is also known that a certain amount of H_2O strongly enhances the H_2 production by photocatalytic dehydrogenation of EtOH [76] allowing, in this case, to reduce the irradiation time required for the complete reduction of the nitro compound.

To avoid a large excess of acetaldehyde during benzimidazole synthesis, the molecular precursor has been changed to 2-nitro aniline (NA), a compound with a much lower toxicity with respect to 1,2-phenylenediamine and producible on a large scale in chemical industry. The results obtained during irradiation of NA in EtOH 96% in the presence of Pt/TiO_2-B,N photocatalyst are presented in Fig. 6b. NA conversion and 2-MBI production start immediately after the beginning of irradiation of the photocatalyst and the reaction proceeds regularly with reduction of nitro group, condensation with acetaldehyde and cyclization/dehydrogenation to 2-MBI. In agreement with GC/MS analysis, UV–vis spectra recorded on the solution at various irradiation times (Fig. S13) show the progressive decrease of the intensity of the band centred around 406 nm related to NA and the concomitant increase on the sharp bands in the range 250–300 nm related to 2-MBI. No H_2 is observed in the gas phase up to 8 h, indicating that hydrogen atoms extracted from ethanol are completely employed for reduction of NA. After 8 h, when NA conversion is around 90%, H_2 begins to be detected in gas phase, with a sharp increase in its concentration. After approximatively 10 h of irradiation, NA is completely converted with a 2-MBI yield close to 100%. Obviously, the time required to reach the complete conversion of NA is almost half of that required in the case on DNB, since NA contains only one nitro group. Only a very minor amount of *N*-Et-2-MBI (0.84 mol%) is detected as by-product. Considering the very high selectivity in 2-MBI synthesis from NA, substituted NA have been employed for the further investigations in the preparation of substituted benzimidazoles.

To highlight the importance of the use of TiO_2-B,N as photoactive support in benzimidazole synthesis, the reaction has been performed also using Pt/TiO_2. Accordingly to the lower H_2 production rates observed for the undoped TiO_2 photocatalysts, 15 h were required to completely convert NA in 2-MBI. Moreover, GC/MS analysis of the procuts mixture revealed that, besides 2-MBI, N-Et-2-MBI and N-EtOEt-2-MBI were present (3.54 mol% and 1.32 mol%, respectively). This result indicates that the use of TiO_2-B,N affects both the H_2 production rate and the following cyclization and dehydrogenation steps required for the synthesis if 2-MBI.

3.4. Photocatalytic synthesis of substituted benzimidazole: influence of metal co-catalyst on selectivity

To extend the photocatalytic approach in the synthesis of more relevant molecules, the synthesis of benzimidazole unit has been performed also using substituted 2-nitro anilines as starting materials. The scope of this investigation was the evaluation of selectivity in benzimidazole production of the various metal co-catalyst employed, with the attempt to preserve the substituents on the aromatic ring for further functionalization of the product. As representative examples, we selected a bromo- and a dichloro-substituted 2-nitroanilines and another one with an ester group. In the first 2 cases, the expected products can be further functionalized by the well-known coupling reactions [77–79] while the ester group in the last one can be easily converted into many other organic functionalities. The experiments have been conducted irradiating the solution on the substituted NA in EtOH 96% at 30 °C in the presence of the TiO_2-B,N photocatalyst loaded with the various metal co-catalysts. Irradiation has been performed until a stable and significant H_2 evolution is observed and UV–vis analysis confirms the complete reduction of the nitro group.

The results obtained with the different co-catalyst in the synthesis of substituted 2-MBI starting from 4-bromo-2-nitro-aniline are presented in Fig. 7, with the GC/MS analysis of the product mixture (after purification from eventual by-products from aldol condensation of acetaldehyde by extraction) are reported in Fig. S14. It's clearly possible to observe that the metal co-catalyst strongly affects the selectivity of the synthesis. Moreover, it must be immediately underlined that the irradiation time required to complete the reaction (complete disappearing of the nitro compound checked by UV–vis and significant and constant H_2 production detected in the gas stream from the reactor) also depends on the nature of metal co-catalyst, in agreement with the H_2 production rates reported in Fig. 4b.

The shorter reaction time is observed for Pt (11.5 h) followed by Pd (14.0 h). This is in agreement with the very high H_2 production observed for Pt/TiO_2-B,N and Pd/TiO_2-B,N. The reason why the reaction time required by Pd/TiO_2-B,N is significantly longer than that of Pt can be explained considering the selectivity of the products. Pt/TiO_2-B,N shows a very high selectivity (93.5%) for 5-bromo-2-methyl-1H-benzimidazole (Br-2-MBI), with only 2-MBI as by-product. In the case of Pd/TiO_2-B,N,

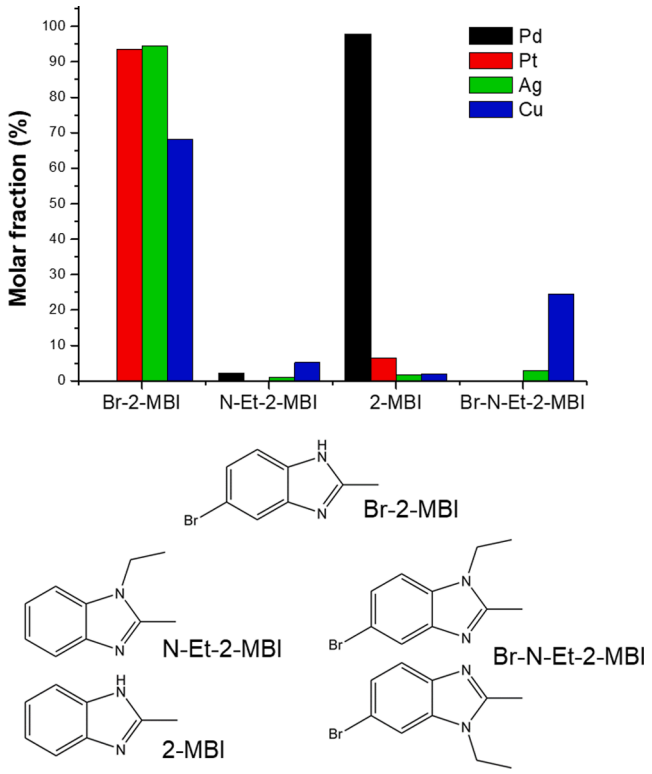

Fig. 7. Effect of metal co-catalyst in the photocatalytic synthesis of 5-bromo-2-methyl-1H-benzimidazole (Br-2-MBI) from 4-bromo-2-nitro-aniline. Experimental condition: 150 mg Pt/TiO_2-B,N, 60 mL solution of precursor 4 mM in EtOH 96%, 30 °C, 30 mL/min Ar flow, simulated sunlight irradiation.

the product produced with 97.8% of selectivity is 2-MBI, indicating that dehydrohalogenation is been performed with a very high efficiency on the Pd nanoparticles. Pd-based heterogeneous catalysts are among the most efficient for hydrodehalogenation of organic substrates following many different strategies: using H_2 gas [80,81], by H-transfer reaction [82] or by electrocatalytic H generation [83]. Beside of synthetic purposes, hydrodehalogenation with Pd-based catalysts have already been reported for the remediation of contaminated soils [84] and abatement of chlorofluorocarbons (CFC) [85]. In the present case, Pd/TiO_2-B,N demonstrated to be highly efficient in removing Br from the aromatic ring during synthesis of benzimidazole, by H-transfer from EtOH. The present results suggest the potentiality of the photocatalytic approach in the hydrodehalogenation of pollutant compounds, using organic renewables (already present in contaminates soils) as sacrificial agents and H donors. From our data, it is evident that Pt has a much lower hydrodehalogenation activity, favouring the reduction of nitro groups instead of breaking of the C-Br bond. These results, together with the possibility to recycle Pd from spent catalysts in a sustainable way [47], make Pd-based photocatalysts among the most promising in pollutant removal.

The irradiation times required for Ag/TiO_2-B,N and Cu/TiO_2-B,N to complete the benzimidazole synthesis (22.0 and 20.5 h, respectively) are in agreement with the lower H_2 production rate observed for these photocatalysts (Fig. 4b). GC/MS analysis of the benzimidazole products shows important differences with respect to the previous photocatalysts. When Ag/TiO_2-B,N is used, the selectivity in the desired product (Br-2-MBI) is comparable with that of Pt/TiO_2-B,N (94.4%) but all the by-products listed in Fig. 7 are observed (Fig. S14). In the case of Cu/TiO_2-B,N, the selectivity for the main product is the lowest observed (68.2%) and high amounts of the by-products are detected. In particular, high amounts of the two isomers of bromo-1-*N*-ethyl-1-methyl-benzimidazole (Br-N-Et-2-MBI) are present. Notably, these compounds are the N-ethyl derivative formed by cyclization the diimine intermediate (Fig. 5): they differ only for the position of the Br substituent on the aromatic ring because they are formed by the nucleophilic attach of N atom of one imino group to the first C atom on the other imino group. Due to their very similar molecular structure, these two compounds cannot be univocally distinguished from their MS spectra and they are counted together in Fig. 7. In comparison with Pd, Ag and Cu show very limited hydrodehalogenation activity but the yields in the N-ethyl derivatives is much higher than that observed for Pt. The production of N-ethyl derivatives could be related with the lower activity of Ag- and Cu-based photocatalysts in the dehydrogenation process, a step that is crucial in producing the desired benzimidazole after cyclization (Fig. 5). In fact, if the intermediate obtained from cyclization is not dehydrogenated/oxidized quickly, it can be subjected to re-opening of the ring and formation of the di-imine intermediate, the precursor of N-ethyl derivate.

Considering the overall performance of the 4 investigated photocatalysts, only Pt and Pd have been have been employed for the prosecution of the study considering that, even if Pd showed the total removal of Br from the product, the N-ethyl by-products are absent. Therefore, Pt/TiO_2-B,N and Pd/TiO_2-B,N have been tested in the synthesis of the benzimidazoles starting from 4,5-dichloro-2-nitro-aniline and from methyl 4-amino-3-nitro-benzoate. The selectivity in the various products are presented in Fig. 8.

In the synthesis of 5,6-dichloro-2-methyl-1H-benzimidazole (diCl-2-MBI) from 4,5-dichloro-2-nitro-aniline, the behaviours of Pt and Pd-based photocatalysts is again significantly different. When using Pt/TiO_2-B,N, the selectivity in the desired product (diCl-2-MBI) is still very high (95.7%) and only a minor amount of 5-chloro-2-methyl-1H-benzimidazole (Cl-2-MBI) was detected. Using Pd/TiO_2-B,N, the selectivity of the desired product is much lower, with the production of large amounts of the by-products Cl-2-MBI and 2-MBI as a result of the hydrodehalogenation reaction. In agreement with this, the irradiation

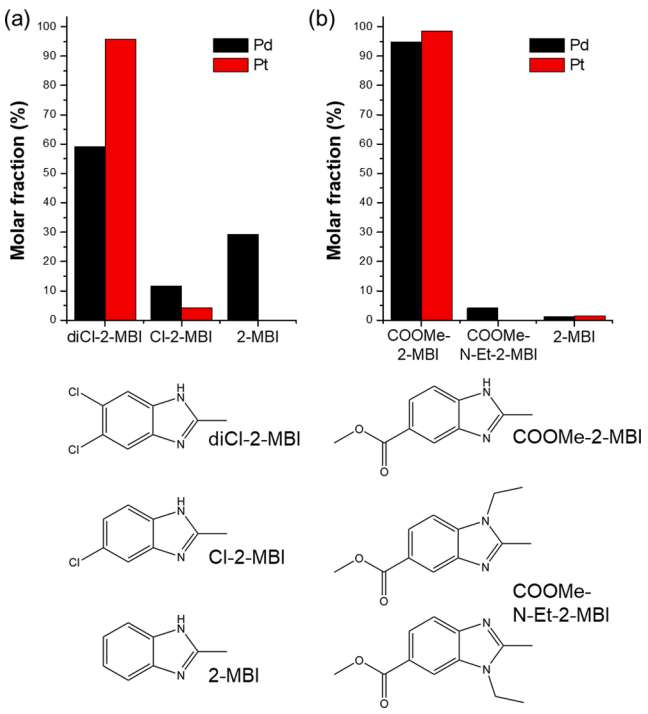

Fig. 8. Effect of metal co-catalyst in the photocatalytic synthesis of (a) 5,6-dichloro-2-methyl-1H-benzimidazole (diCl-2-MBI) from 4,5-dichloro-2-nitro-aniline and (b) 5-carboxymethyl-2-methyl-1H-benzimidazole (COOMe-2-MBI) from methyl 4-amino-3-nitro-benzoate. Experimental condition: 150 mg Pt/TiO_2-B,N, 60 mL solution of precursor 4 mM in EtOH 96%, 30 °C, 30 mL/min Ar flow, simulated sunlight irradiation.

time required for the complete conversion of the nitro aniline is much longer using Pd/TiO_2-B,N (13.0 h) than using Pt/TiO_2-B,N (11.5 h). The observed differences in the selectivity is again related with the ability of Pt and Pd to promote the reduction of nitro groups over the hydrodehalogenation, in agreement with the results previously reported for the selective catalytic hydrogenation of nitro groups in the presence of activated aryl halides [86]. The GC/MS analysis of the product mixtures obtained from 4,5-dichloro-2-nitro-aniline are presented in Fig. S15.

Finally, in the synthesis of 5-carboxymethyl-2-methyl-1H-benzimidazole from methyl 4-amino-3-nitro-benzoate both Pt/TiO_2-B,N and Pd/TiO_2-B,N show very high selectivity to the desired product (98.5% and 94.7%, respectively). In the case of Pt/TiO_2-B,N, GC/MS analysis revealed the presence of only a very low amount of 2-MBI, indicating that the ester group has been completely removed from the product. On the other hand, using Pd/TiO_2-B,N relevant amounts on the N-ethyl derivatives has been detected (Fig. S1). Again, the two isomers cannot be distinguished only on the basis of their MS spectra and are quantified together.

4. Conclusions

In this work, we investigated the role of co-doping of TiO_2 with B and N and of the employed co-catalyst on the photocatalytic activity of the obtained materials in H_2 production by dehydrogenation of ethanol and its use for the production of 2-methylbenzimidazole by a one-pot process starting from non-toxic nitroaniline compounds. Co-coping of TiO_2 increases surface area of TiO_2 by significantly reducing the crystallite sizes without affecting the phase composition of the materials. The H_2 production rate is favourable influenced by this increase of surface area while the various metal co-catalysts (Pt, Pd, Cu, Ag) are affecting the photocatalytic performance accordingly to their work function.

Photocatalytic 2-MBI synthesis has been optimized starting from dinitrobenzene or 2-nitro aniline, showing that a low amount of H_2O in the solvent is convenient to avoid formation of highly toxic intermediates (such as phenylenediamine) or of un-desired N-substituted benzimidazoles. The synthesis of 2-MBI proceeds through reduction of the nitro groups by the H abstracted from ethanol by the photocatalyst, reaction of amino groups with the acetaldehyde and rapid cyclization of the imine intermediate, which produces the 2-MBI after oxidation/dehydrogenation.

The metal loaded co-catalysts have been investigated also in the synthesis of substituted benzimidazoles. The best performance of Pt/TiO_2-B,N in benzimidazole synthesis derive from a combination of two factors. The first is the high activity in H_2 production, which reduces the time required for complete reduction of nitro groups. The second factor is the low ability of Pt to hydrogenate the C-Cl and C-Br bonds in halogen-substituted precursors or the C—O bond in the esther-functionalized precursor. These aspects are now better summarized in the conclusion section. Cu and Ag showed the production of large amounts of N-ethyl benzimidazole products while Pd is able to efficiently promote the hydrodehalogenation of the aromatic ring. Despite this result could be useful for other applications (like degradation of halogenated environmental pollutants), in this case halogens must be preserved for further functionalization of the products. The study clearly indicate the potentiality of metal loaded photocatalysts for organic synthesis and of benzimidazole in particular. However, a fine tuning of the nature of the metal co-catalyst, of the properties of the semiconductor, from its surface area, light absorption characteristic and acidic nature, is necessary to guaranty promising activity and selectivity.

Declaration of Competing Interest

The authors declare that they have no known competing financial interests or personal relationships that could have appeared to influence the work reported in this paper.

Acknowledgements

TM, GC, GA, and PF acknowledge the University of Trieste (FRA 2018), Ministry for University and Research (PRIN 2017PBXPN4), INSTM Consortium and ICCOM-CNR for financially supporting their research activities. JJD thanks the financial support of the Ministry of Science and Innovation of Spain/FEDER Program of the EU (ENE2017-82451-C3-2-R).

Appendix A. Supplementary data

Supplementary data to this article can be found online at https://doi.org/10.1016/j.ica.2021.120289.

References

[1] United Nation, 17 Sustain. Delevopment Goals (n.d.) https://sdgs.un.org/.
[2] G. Palmisano, V. Augugliaro, M. Pagliaro, L. Palmisano, Chem. Commun. (Camb). (2007) 3425–3437.
[3] J.J. Douglas, M.J. Sevrin, C.R.J. Stephenson, Org. Process Res. Dev. 20 (2016) 1134–1147.
[4] T.P. Nicholls, D. Leonori, A.C. Bissember, Nat. Prod. Rep. 33 (2016) 1248–1254.
[5] A.V. Puga, Coord. Chem. Rev. 315 (2016) 1–66.
[6] I. Romero Ocaña, A. Beltram, J.J. Delgado Jaén, G. Adami, T. Montini, P. Fornasiero, Inorganica Chim. Acta 431 (2015) 197–205.
[7] M. Cargnello, A. Gasparotto, V. Gombac, T. Montini, D. Barreca, P. Fornasiero, Eur. J. Inorg. Chem. (2011) 4309–4323.
[8] M.F. Kuehnel, E. Reisner, Angew. Chemie Int. Ed. 57 (2018) 3290–3296.
[9] N. Luo, T. Montini, J. Zhang, P. Fornasiero, E. Fonda, T. Hou, W. Nie, J. Lu, J. Liu, M. Heggen, L. Lin, C. Ma, M. Wang, F. Fan, S. Jin, F. Wang, Nat. Energy 4 (2019) 575–584.
[10] F. Su, S.C. Mathew, G. Lipner, X. Fu, M. Antonietti, S. Blechert, X. Wang, J. Am. Chem. Soc. 132 (2010) 16299–16301.
[11] A. Tanaka, K. Hashimoto, H. Kominami, J. Am. Chem. Soc. 134 (2012) 14526–14533.
[12] S. Higashimoto, N. Kitao, N. Yoshida, T. Sakura, M. Azuma, H. Ohue, Y. Sakata, J. Catal. 266 (2009) 279–285.
[13] J. Diniz, C.D. Nunes, O.C. Monteiro, Inorg. Chem. Commun. 119 (2020), 108099.
[14] X. Lin, S. Xu, Z.Q. Wei, S. Hou, Q.L. Mo, X.Y. Fu, F.X. Xiao, J. Mater. Chem. A 8 (2020) 20151–20161.
[15] Y. Wang, X. Wang, M. Antonietti, Angew. Chemie - Int. Ed. 51 (2012) 68–89.
[16] Q. Xiao, S. Sarina, E.R. Waclawik, J. Jia, J. Chang, J.D. Riches, H. Wu, Z. Zheng, H. Zhu, ACS Catal. 6 (2016) 1744–1753.
[17] H. Wang, J. Yan, W. Chang, Z. Zhang, Catal. Commun. 10 (2009) 989–994.
[18] Z. Ding, X. Chen, M. Antonietti, X. Wang, ChemSusChem 4 (2010) 274–281.
[19] X.H. Li, M. Baar, S. Blechert, M. Antonietti, Sci. Rep. 3 (2013) 1–6.
[20] S. Zhang, C. Chang, Z. Huang, Y. Ma, W. Gao, J. Li, Y. Qu, ACS Catal. 5 (2015) 6481–6488.
[21] A. Savateev, I. Ghosh, B. König, M. Antonietti, Angew. Chemie - Int. Ed. 57 (2018) 15936–15947.
[22] M. Boiani, M. Gonzalez, Mini-Rev. Med. Chem. 5 (2005) 409–424.
[23] P.S. Charifson, A.L. Grillot, T.H. Grossman, J.D. Parsons, M. Badia, S. Bellon, D. D. Deininger, J.E. Drumm, C.H. Gross, A. LeTiran, Y. Liao, N. Mani, D.P. Nicolau, E. Perola, S. Ronkin, D. Shannon, L.L. Swenson, Q. Tang, P.R. Tessier, S.K. Tian, M. Trudeau, T. Wang, Y. Wei, H. Zhang, D. Stamos, J. Med. Chem. 51 (2008) 5243–5263.
[24] A.W. White, R. Almassy, A.H. Calvert, N.J. Curtin, R.J. Griffin, Z. Hostomsky, K. Maegley, D.R. Newell, S. Srinivasan, B.T. Golding, J. Med. Chem. 43 (2000) 4084–4097.
[25] G. Rackur, M. Bickel, H.W. Fehlhaber, A. Herling, V. Hitzel, H.J. Lang, M. Rösner, R. Weyer, Biochem. Biophys. Res. Commun. 128 (1985) 477–484.
[26] D. Luneau, P. Rey, Coord. Chem. Rev. 249 (2005) 2591–2611.
[27] F. Téllez, H. López-Sandoval, S.E. Castillo-Blum, N. Barba-Behrens, Arkivoc 2008 (2008) 245–275.
[28] Y. Dong, H. Zhang, F. Lei, M. Liang, X. Qian, P. Shen, H. Xu, Z. Chen, J. Gao, J. Yao, J. Solid State Chem. 245 (2017) 160–163.
[29] P.N. Preston, Chemical Reviews Synthesis, Reactions, and Spectroscopic Properties of Benzimidazoles, 1974.
[30] J.B. Wright, Chem. Rev. 48 (1951) 397–541.
[31] S.I. Alaqeel, J. Saudi Chem. Soc. 21 (2017) 229–237.
[32] K. Bahrami, M.M. Khodaei, I. Kavianinia, Synthesis 2007 (2007) 547–550.
[33] P.L. Beaulieu, B. Haché, E. Von Moos, Synthesis 2003 (2003) 1683–1692.
[34] Y. Shiraishi, Y. Sugano, S. Tanaka, T. Hirai, Angew. Chemie - Int. Ed. 49 (2010) 1656–1660.
[35] K. Selvam, M. Swaminathan, Tetrahedron Lett. 52 (2011) 3386–3392.
[36] T. Montini, M. Monai, A. Beltram, I. Romero-Ocaña, P. Fornasiero, Mater. Sci. Semicond. Process. 42 (2016) 122–130.
[37] K.C. Christoforidis, T. Montini, M. Fittipaldi, J.J.D. Jaén, P. Fornasiero, ChemCatChem 11 (2019) 6408–6416.
[38] T. Montini, V. Gombac, L. Sordelli, J.J. Delgado, X. Chen, G. Adami, P. Fornasiero, ChemCatChem 3 (2011) 574–577.

[39] V. Gombac, L. Sordelli, T. Montini, J.J. Delgado, A. Adamski, G. Adami, M. Cargnello, S. Bernai, P. Fornasiero, J. Phys. Chem. A 114 (2010).
[40] M. Melchionna, A. Beltram, T. Montini, M. Monai, L. Nasi, P. Fornasiero, M. Prato, Chem. Commun. 52 (2016) 764–767.
[41] A. Beltram, M. Melchionna, T. Montini, L. Nasi, P. Fornasiero, M. Prato, Green Chem. 19 (2017) 2379–2389.
[42] M. Cargnello, T. Montini, S.Y. Smolin, J.B. Priebe, J.J. Delgado Jaén, V.V.T. Doan-Nguyen, I.S. McKay, J.A. Schwalbe, M.-M. Pohl, T.R. Gordon, Y. Lu, J.B. Baxter, A. Brückner, P. Fornasiero, C.B. Murray, Proc. Natl. Acad. Sci. 113 (2016) 3966–3971.
[43] A. Gallo, T. Montini, M. Marelli, A. Minguzzi, V. Gombac, R. Psaro, P. Fornasiero, V. Dal Santo, ChemSusChem 5 (2012) 1800–1811.
[44] A. Beltram, I. Romero-Ocaña, J.J. Delgado Jaen, T. Montini, P. Fornasiero, J. Josè Delgado Jaen, T. Montini, P. Fornasiero, Appl. Catal. A Gen. 518 (2016) 167–175.
[45] M. Murdoch, G.I.N. Waterhouse, M.A. Nadeem, J.B. Metson, M.A. Keane, R. F. Howe, J. Llorca, H. Idriss, Nat. Chem. 3 (2011) 489–492.
[46] A. Naldoni, T. Montini, F. Malara, M.M. Mróz, A. Beltram, T. Virgili, C.L. Boldrini, M. Marelli, I. Romero-Ocaña, J.J. Delgado, V. Dal Santo, P. Fornasiero, ACS Catal. 7 (2017) 1270–1278.
[47] V. Gombac, T. Montini, A. Falqui, D. Loche, M. Prato, A. Genovese, M.L. Mercuri, A. Serpe, P. Fornasiero, P. Deplano, Green Chem. 18 (2016) 2745–2752.
[49] C. Di Valentin, G. Pacchioni, Catal. Today 206 (2013) 12–18.
[50] G. Liu, Y. Zhao, C. Sun, F. Li, G.Q. Lu, H.-M. Cheng, Angew. Chem. Int. Ed. Engl. 47 (2008) 4516–4520.
[51] V. Gombac, L. De Rogatis, A. Gasparotto, G. Vicario, T. Montini, D. Barreca, G. Balducci, P. Fornasiero, E. Tondello, M. Graziani, Chem. Phys. 339 (2007) 111–123.
[52] K.S.W. Sing, D.H. Everett, R.A.W. Haul, L. Moscou, R.A. Pierotti, J. Rouquerol, T. Siemieniewska, Pure Appl Chem 57 (1985) 603–619.
[53] A. Zaleska, E. Grabowska, J.W. Sobczak, M. Gazda, J. Hupka, Appl. Catal. B Environ. 89 (2009) 469–475.
[54] R. Asahi, T. Morikawa, H. Irie, T. Ohwaki, Chem. Rev. 114 (2014) 9824–9852.
[55] A. V. Puga, N. Barka, M. Imizcoz, ChemCatChem (2020) cctc.202001048.
[57] A.V. Puga, A. Forneli, H. García, A. Corma, Adv. Funct. Mater. 24 (2014) 241–248.
[58] A. Petala, E. Ioannidou, A. Georgaka, K. Bourikas, D.I. Kondarides, Appl. Catal. B Environ. 178 (2015) 201–209.
[59] V. Polliotto, S. Livraghi, A. Krukowska, M.V. Dozzi, A. Zaleska-Medynska, E. Selli, E. Giamello, A.C.S. Appl, Mater. Interfaces 10 (2018) 27745–27756.
[60] Z. Wang, K. Teramura, T. Shishido, T. Tanaka, in: Top. Catal., Kluwer Academic Publishers, 2014, pp. 975–983.
[61] M. Imizcoz, A.V. Puga, Catal. Sci. Technol. 9 (2019) 1098–1102.
[62] C.A. Emilio, M.I. Litter, M. Kunst, M. Bouchard, C. Colbeau-Justin, Langmuir 22 (2006) 3606–3613.
[63] J.T. Carneiro, T.J. Savenije, J.A. Moulijn, G. Mul, J. Phys. Chem. C 115 (2011) 2211–2217.
[64] Y. Liu, Z. Wang, W. Wang, W. Huang, J. Catal. 310 (2014) 16–23.
[65] C.-H. Lin, C.-H. Lee, J.-H. Chao, C.-Y. Kuo, Y.-C. Cheng, W.-N. Huang, H.-W. Chang, Y.-M. Huang, M.-K. Shih, Catal. Lett. 98 (2004) 61–66.
[66] H.-L. Kuo, C.-Y. Kuo, C.-H. Liu, J.-H. Chao, C.-H. Lin, Catal. Letters 113 (2007) 7–12.
[67] M.V. Dozzi, E. Selli, J. Photochem. Photobiol. C Photochem. Rev. 14 (2013) 13–28.
[68] Y. Li, G. Ma, S. Peng, G. Lu, S. Li, Appl. Surf. Sci. 254 (2008) 6831–6836.
[69] H. Kisch, D. Bahnemann, J. Phys. Chem. Lett. 6 (2015) 1907–1910.
[70] B. Gupta, A.A. Melvin, T. Matthews, S. Dash, A.K. Tyagi, Renew. Sustain. Energy Rev. 58 (2016) 1366–1375.
[71] Y. Mizukoshi, Y. Makise, T. Shuto, J. Hu, A. Tominaga, S. Shironita, S. Tanabe, Ultrason. Sonochem. 14 (2007) 387–392.
[72] A. Naldoni, M. D'Arienzo, M. Altomare, M. Marelli, R. Scotti, F. Morazzoni, E. Selli, V. Dal Santo, Appl. Catal. B Environ. 130–131 (2013) 239–248.
[74] M. Yasuda, T. Matsumoto, T. Yamashita, Renew. Sustain. Energy Rev. 81 (2018) 1627–1635.
[75] S. Escobedo Salas, B. Serrano Rosales, H. De Lasa, Appl. Catal. B Environ. 140–141 (2013) 523–536.
[76] N. Strataki, V. Bekiari, D.I. Kondarides, P. Lianos, Appl. Catal. B Environ. 77 (2007) 184–189.
[77] A. Suzuki, Angew. Chemie - Int. Ed. 50 (2011) 6722–6737.
[78] I.P. Beletskaya, F. Alonso, V. Tyurin, Coord. Chem. Rev. 385 (2019) 137–173.
[79] E.I. Negishi, Angew. Chemie - Int. Ed. 50 (2011) 6738–6764.
[80] C.-H. Pélisson, A. Denicourt-Nowicki, C. Meriadec, J.-M. Greneche, A. Roucoux, ChemCatChem 7 (2015) 309–315.
[81] H. Min, S. Lee, M. Park, J. Hwang, H.M. Jung, S. Lee, J. Organomet. Chem. 755 (2014) 7–11.
[82] M. Muzzio, H. Lin, K. Wei, X. Guo, C. Yu, T. Yom, Z. Xi, Z. Yin, S. Sun, A.C. S. Sustain, Chem. Eng. 8 (2020) 2814–2821.
[83] C. Cui, J. Wu, Y. Xin, Y. Han, Korean J. Chem. Eng. 32 (2015) 1069–1074.
[84] H.Y. Wee, J. Cunningham, Environ. Prog. Sustain Energy 30 (2011) 589–598.
[85] S.C. Shekhar, J.K. Murthy, P.K. Rao, K.S.R. Rao, Appl. Catal. A Gen. 271 (2004) 95–101.
[86] A.J. Kasparian, C. Savarin, A.M. Allgeier, S.D. Walker, J. Org. Chem. 76 (2011) 9841–9844.